Climatological Aspects of Radiation Fog Occurrence at Albany, New York

MICHAEL B. MEYER AND G. GARLAND LALA

Atmospheric Sciences Research Center, State University of New York at Albany, Albany, New York

(Manuscript received 6 September 1988, in final form 28 November 1989)

ABSTRACT

We present a detailed investigation of the local radiation fog climatology, carried out in support of our ongoing field program to study radiation fog mechanisms at Albany, New York. At Albany, a distinct "radiation fog season" is observed during September and October. We show that this late-summer/early-autumn maximum in radiation fog observations is primarily due to a sufficient period of nocturnal cooling coupled with an adequate moisture supply. Five critical surface synoptic patterns are responsible for initiating the radiation fog process. In addition, radiation fog life cycles are generally confined to a modest time window centered on sunrise. Key parameters necessary for forecasting the onset time of fog are shown to be the initial relative humidity and nocturnal cooling rate.

1. Introduction

In support of an ongoing field program to study radiation fog mechanisms at Albany, New York (Meyer et al. 1986), a detailed investigation of the local radiation fog climatology was undertaken. The primary goal was to determine the character and predictability of these radiation fogs using the standard local climate data. The results, with particular emphasis on fog season identification, synoptic patterns, diurnal characteristics and implications for forecasting, are presented here.

The accurate forecasting of fog events requires a familiarity with fog climatology and local meteorology. The most recent presentations of fog frequency distributions over the United States have delineated general large-scale annual (Court and Gerston 1966; Peace 1969) and monthly (Hardwick 1973) fog trends. While these reports are useful for distinguishing the geographical occurrence of fog, they do not address the mechanisms responsible. Some attention has been given to the identification and geographical distribution of dominant fog types (e.g., radiation, advection, frontal—see section 2 for further discussion) within the contiguous United States (Stone 1936; George 1940; Willett 1944; Byers 1959). These studies, however, lack sufficient detail to be of practical use in a local daily fog forecast scheme.

Depending on the fog type present, fog droplets can range in size from 5 to 65 μm diameter, fog thickness can vary from very shallow to over 300 meters, and surface visibility can often differ by a factor of two or more (Jiusto 1981). An increased understanding of local climatological parameters associated with a specific fog type appears to carry some benefit. This would presumably allow better recognition and more accurate forecasting of the situations most suitable for a certain fog type to occur. At Albany, radiation fogs are predominant, and are the focus of this work.

2. Database and procedure

The ten year period of 1970 to 1979 was selected for compiling a local fog climatology for Albany. The Local Climatological Data (LCD) monthly summaries, surface weather observation (SWO) forms MF1-10A and MF1-10B, and the North American surface weather maps available from the National Climatic Data Center, National Oceanic and Atmospheric Administration, were used as the primary database. The LCDs and SWOs were collected for the National Weather Service (NWS) site at the Albany County Airport. This NWS station is located at 42.75°N, 73.8°W, near the confluence of the Mohawk (site is ~3 km to the south) and Hudson (~10 km to the west) rivers.

By surveying the LCDs for the decade, an initial dataset of 215 "heavy" fog days was assembled. Heavy fog is defined as fog with a surface prevailing visibility of 400 m or less, and is indicated on the LCD as weather type 2 under the column heading "Weather Types on Dates of Occurrence." For the remainder of the text the term "fog" will imply "heavy fog" when referring to climatological data. Next, using the SWOs, a distinction was drawn between a fog day and a fog event. This was done to account for the variable nature of fog and avoid multiple counting of the same fog event. Once the surface prevailing visibility fell to the fog

Corresponding author address: Michael B. Meyer, 17 Miles Standish Road, Schenectady, NY 12306.

© 1990 American Meteorological Society

Unauthenticated | Downloaded 03/22/23 05:50 AM UTC

threshold, a fog event was considered to be in progress. Criteria (arbitrary) for determining the end of the fog event were: 1) visibility greater than or equal to 1.6 km for 12 or more hours, or 2) visibility greater than or equal to 3.2 km for 6 or more hours. Thus, it is possible for a fog event to encompass one or more periods of fog and span more than one day. The fog frequency studies of Court and Gerston (1966), Peace (1969), and Hardwick (1973) all used the fog day. The use here of the fog event instead of the fog day reduces the database by 6.5% (201 events). The event approach to describing the local fog climatology provides a more realistic view since synoptic phenomena are not constrained by the midnight time boundary.

The SWOs were also used to determine fog character and record concurrent synoptic conditions. Both hourly (record) and special observations were used. Although record observations are reported on the hour, the actual time of the observation is often 10 to 20 minutes earlier. No adjustment has been made for this. Our assessment of fog character includes the total hours of fog, minimum visibility, and the extent of visibility degradation to at least 100 m. In order to determine fog duration in minutes, measurements at the time of observation were assumed unchanged until the time of the next observation. The surface temperature and pressure, resultant and average winds, current and prior precipitation, and snow cover, were logged for each fog event.

The next step was to determine which were radiation fog events. Radiation fog formation depends upon a critical balance between nocturnal longwave radiational cooling and the turbulent diffusion of heat and moisture in the surface layer. Taylor (1917) was perhaps the first to recognize this physical foundation for radiation fog development. Using Taylor's concept, Willett (1928) postulated that some dynamic turbulence helped extend the ground cooling (produced by radiational cooling) into the surface layer, while still preserving the surface temperature inversion. Later, Emmons and Montgomery (1947) recognized that cooling by radiative flux divergence in the air itself must also be included in the fog formation theory. The presence of cloud cover acts to inhibit the cooling necessary to saturate the air, while excessive wind speed promotes drying of the air and reduces the cooling rate of the surface layer. Thus, meteorological conditions favorable for the onset of radiation fog must necessarily include thinning, clearing, or absence of cloud cover, minimal wind speed, and falling air temperature due to nocturnal radiational cooling.

Using these broad guidelines, along with the SWOs, one can draw a clear distinction between radiation (143 cases) and nonradiation (58 cases) fog events. Nonradiation fog types found included frontal, precipitation, and advection fog. At Albany, frontal fogs are primarily a result of stratus lowering accompanying a cold frontal passage, and may or may not be associated with precipitation. Precipitation fogs are those associated with drizzle, rain, or snow, while advection fogs are due to the transport of warmer moist air over a colder (i.e., snow covered) surface.

An anticyclonic surface synoptic pattern often results in the meteorological criteria necessary for radiation fog. George (1951) cites restricted heating and air drainage as two primary scenarios favorable for radiation fog. The restricted heating scenario assumes that the local air has been under a cloud cover (with or without precipitation) during the day previous to its formation. This is often the case with postfrontal anticyclonic ridging and frontolysis. Air-drainage fog arises from cool air collecting in valleys, such as river valleys, and is predominantly due to the influence of a large scale high pressure cell or ridge. The appropriate North American surface maps were used to determine which synoptic patterns prevailed during the radiation fog events.

3. Radiation fog season

a. Identification

Figure 1a shows the monthly frequency of radiation fog events per year averaged over the 10 year observation period at Albany. A distinct late-summer/early-autumn "radiation fog season" is apparent, with more than half of the fog events concentrated in the months of September and October. No fog events occurred in December. By season, radiation fogs are most prevalent in the autumn (September, October, November) with 65.0% of the total, followed by summer (June, July, August—23.8%), spring (March, April, May—8.4%) and wintertime (December, January, February—2.8%). The observed September–October maximum agrees well with the published data of Stone (1936) for northeastern radiation fogs.

The ratio of radiation fog events to all fog-type events is plotted versus month in Fig. 1b. Note that there is an autumnal peak in radiation fog percentage, with nearly all fogs in September and October being of the radiation type. This peak, however, is much broader than that of Fig. 1a. During the winter and early spring radiation fogs are relatively rare (13.2%). A gradual increase in percentage is indicated following March, with well over 80% of all fog events being radiation-type during the months of June through October. At Albany, 71% of all fog events are radiation fogs.

One measure of the radiation fog character is given by the monthly frequency of the fog event duration, plotted in Fig. 1c, where the duration is indicated as the mean number of hours of fog per event. A trend toward a summer minimum, as well as an autumnal and a late-winter/early-spring maxima, is apparent, although the February–March maximum is based on few events. In general, during the Albany radiation fog season, one can expect fogs of 3 to 4 hour duration.

Unauthenticated | Downloaded 03/22/23 05:50 AM UTC

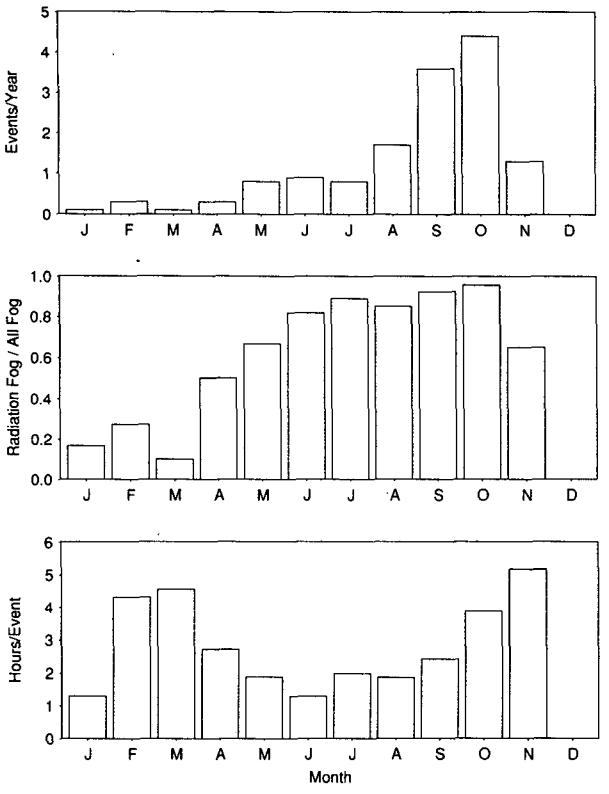

FIG. 1. Monthly frequency of (a) heavy (visibility ≤ 400 m) radiation fog events per year, (b) ratio of the number of heavy radiation fog events to all heavy radiation fog events, (c) number of hours of heavy radiation fog per event. Climate data are for Albany, New York, 1970–79.

b. *Physical model*

A late-summer/early-autumn maximum in the radiation fog frequency is primarily due to a sufficient amount of hours available for nocturnal cooling, coupled with an adequate moisture supply. We postulate that a simple surface layer model can be formulated to estimate the time necessary to produce a radiation fog. Using standard mean monthly climatological weather observations (from LCDs), this predicted time, relative to the length of night, will explain the observed seasonal trend of Albany radiation fog occurrence.

If we assume that the specific humidity (q) of the air and the total atmospheric pressure (p) remain nearly constant through the night, then, by definition of the saturation specific humidity ($q_s \approx \epsilon e_s/p$, where e_s is the saturation vapor pressure) and by using the Clausius–Clapeyron equation ($de_s/dT = \epsilon L_v e_s/RT^2$), the time rate of change of the saturation deficit can be specified by

$$\frac{\partial(q_s - q)}{\partial t} \approx \frac{\partial q_s}{\partial t} \approx \frac{\epsilon}{p}\frac{de_s}{dT}\frac{\partial T}{\partial t} \approx q_s \frac{\epsilon L_v}{RT^2}\frac{\partial T}{\partial t} \quad (1)$$

where $\epsilon = 0.622$, L_v is the latent heat of vaporization of water, R is the dry air gas constant, and T is the absolute temperature. In the development of Eq. (1) we have also assumed that q is approximately equal to the mixing ratio, vapor pressure is negligible when compared with p, and L_v is independent of temperature. The constant q assumption is supported by the monthly mean climate data, which indicate that the change in q through an evening is roughly one-tenth that of q_s. With a constant cooling rate, $\partial T/\partial t$, Eq. (1) may be integrated from the initial saturation specific humidity, q_{s0}, to the final value at saturation, q. The function $1/T^2$ varies less than 10% over the temperature fall of the night, and is also held constant. An expression for the time it takes to reach saturation, τ, results:

$$\tau \approx \frac{\dfrac{RT^2}{\epsilon L_v}\ln(\mathrm{RH}_0)}{\dfrac{\partial T}{\partial t}} \quad (2)$$

where RH_0 is the relative humidity at the initiation of the saturation process.

The computation of τ depends most critically on the ratio of the logarithm of the relative humidity over the cooling rate. Thus, a high initial relative humidity combined with strong cooling allows the surface layer to saturate relatively quickly; τ alone, however, is not sufficient to explain the seasonal fog trend. The amount of time it takes to complete the saturation process is quite clearly limited by the length of night (LON). Positive values of τ relative to the LON (τ–LON) indicate that the nighttime is too short to allow the surface layer to saturate, while negative values suggest enough time is available. A direct consequence of the delicate balance between τ and LON is that many of the fogs at Albany form near sunrise (discussed later in section 5).

An independent test of the physical model's ability to discriminate between fog and nonfog conditions, as well as predict the onset time of fog, was achieved using continuous meteorological data from 34 nocturnal cooling cases during our radiation fog field experiments. Time-series plots of temperature, relative humidity, and net radiation made during our field experiments show that the cooling process is initiated near sunset as outgoing longwave radiation begins to dominate. The cooling rate was, therefore, based on the sunset to 0400 LST temperature change, while the 0100 LST temperature was used as the mean for the night. This choice of times allowed for continuity in comparison with the available climate data presented later in this section.

Predicted [τ_p from Eq. (2)] and observed (τ_o) values of τ–LON are shown in Table 1. Note that the cases are grouped by categories; no fog, fog patches, and fog. We considered a fog episode to occur when the measured (with an AEG integrating nephelometer) visual range fell below 1 km. A fog patch case is characterized

Unauthenticated | Downloaded 03/22/23 05:50 AM UTC

TABLE 1. Values of τ_p–LON (predicted) and τ_o–LON (observed) [in decimal hours] for experiments conducted during radiation fog field studies.

Day	Time predicted (τ_p–LON)	Time observed (τ_o–LON)	
		Patches	Fog
	No fog		
11, 12 Oct 1981	−1.01	—	—
13, 14 Sep 1982	1.73	—	—
22, 23 Sep 1982	3.70	—	—
28, 29 Sep 1982	−3.80	—	—
28, 29 Oct 1982	−6.01	—	—
16, 17 Oct 1985	0.10	—	—
17, 18 Oct 1985	−2.70	—	—
	Fog patches		
5, 6 Oct 1981	−9.35	−4.95	—
4, 5 Sep 1982	−3.92	−4.40	—
8, 9 Sep 1982	−3.50	−4.45	—
9, 10 Sep 1982	−7.02	−8.48	—
10, 11 Sep 1982	−2.77	−5.50	—
14, 15 Sep 1982	0.20	−1.07	—
17, 18 Sep 1982	−5.52	−8.57	—
21, 22 Sep 1982	−6.11	−1.70	—
4, 5 Oct 1982	−6.16	−5.95	—
5, 6 Oct 1982	−8.79	−9.95	—
27, 28 Oct 1982	−7.82	−8.40	—
29, 30 Sep 1985	−8.93	−5.35	—
11, 12 Oct 1985	−2.22	−1.08	—
Mean	−5.53	−5.37	—
σ	(2.93)	(2.93)	(—)
	Fog		
10, 11 Oct 1981	−7.03	−9.55	−3.05
12, 13 Oct 1981	−6.47	−10.08	−2.58
13, 14 Oct 1981	−6.94	−9.62	−3.87
25, 26 Sep 1982	−9.36	−7.77	−4.77
29, 30 Sep 1982	−9.34	−7.85	−2.60
30 Sep, 1 Oct 1982	−10.14	−10.87	−1.87
2, 3 Oct 1982	−6.20	−5.90	−1.40
6, 7 Oct 1982	−8.45	−9.98	−1.23
10, 11 Oct 1982	−7.37	−9.05	−5.05
24, 25 Oct 1982	−5.64	−6.00	−0.83
26, 27 Oct 1982	−1.80	−2.37	0.63
20, 21 Oct 1985	−8.88	−5.75	−1.42
21, 22 Oct 1985	−5.63	−6.28	−4.28
22, 23 Oct 1985	−6.72	−5.78	−4.45
Mean	−7.14	−7.63	−2.63
σ	(2.12)	(2.38)	(1.70)

by one or more fog episodes, each lasting less than 1 hour, whereas a fog case contained at least one fog episode of at least 1 hour. The "time observed" column is split into time when patches were first observed, and the beginning time for the extended period of fog. The model predicted surface layer saturation (indicated by negative τ_p–LON) in all but one of the 27 "fog patches" and "fog" experiments. Over 60% of the model predictions were within 2 hours of the observed onset of fog patches. Mean time values suggest that the model predictions are a reasonable indicator of when fog patches will first appear, and that extended spans of fog are generally preceded by fog patches some 5 hours earlier. Also, model forecasts of saturation occuring earlier in the evening tend to be associated with extended fog events. Less than half of the "no fog" cases were predicted by the model (indicated by positive τ_p–LON). It is encouraging, however, that while the model favors saturation for some of the "no fog" cases, it expects this to occur much later in the evening than for the fog cases.

Mean monthly values of standard climatological data (Table 2) were used for the calculation of τ from Eq. (2). The mean monthly temperature and humidity are reported on the LCDs at 3-hour intervals. The estimated temperature and relative humidity values at sunset were obtained by interpolation on a cubic spline fit to these parameters at 1600, 1900, and 2200 LST. Note, however, that the mean monthly values used for input are representative of all nighttime synoptic situations encountered, not just radiation fog patterns. For example, the mean monthly cooling rates are highly dependent on the mean monthly values for cloud cover, net radiation, and wind speed.

Figure 2 shows the monthly frequency of τ–LON (black bars). The graph compares favorably with the observed fog frequency from Fig. 1a, showing a greater tendency toward saturation during the late summer/early autumn. Note that both τ and LON show similar seasonal trends, with a late spring/summer minimum and December maximum (see Table 2). From June through September, τ remains fairly constant. This behavior in τ is primarily a result of a slightly increasing initial relative humidity and decreasing cooling rate over these four months. During the same period, the LON increases more rapidly than τ. These subtle differences in the monthly values of τ and LON account for the presence of the radiation fog season at Albany.

One apparent inconsistency is a secondary minimum in τ–LON during January and February. This can be partially explained employing Petterssen's (1940) mist interval idea. Petterssen states that producing a fog is not only a saturation process, but a condensation process as well. In our Albany radiation fogs we have measured liquid water contents of the order of 0.1 g m^{-3} at the heavy fog threshold. The amount of isobaric cooling necessary to produce this amount of condensed water can be calculated and then used to get a correction to τ. We assume that saturation was reached at 0400 LST, and base the effective cooling rate at that time on the temperature change from 0100 LST to 0400 LST. The time to fog, τ_f, relative to the LON is shown on Fig. 2 (white bars). The tendency to favor fog formation in the late-summer/early-autumn is still apparent, while the comparatively low supply of moisture during the winter months aids in making fog occurrence less likely.

Unauthenticated | Downloaded 03/22/23 05:50 AM UTC

TABLE 2. Monthly mean climate data used for the computation of τ, 1970–79, Albany, New York.

	T (°C) (0100 LST)	RH_o (sunset)	$\partial T/\partial t$ (°C/h) (sunset–0400)	$\partial T/\partial t$ (°C/h) (0100–0400)	LON (hr)	τ (hr)
Jan	−7.6	0.66	−0.36	−0.19	14.57	15.19
Feb	−6.4	0.61	−0.44	−0.33	13.47	14.60
Mar	−0.8	0.60	−0.44	−0.24	12.08	15.95
Apr	4.3	0.53	−0.67	−0.43	10.62	13.57
May	10.8	0.61	−0.69	−0.43	9.38	10.52
Jun	15.2	0.68	−0.70	−0.43	8.74	8.63
Jul	17.5	0.66	−0.75	−0.37	9.02	8.65
Aug	17.0	0.70	−0.64	−0.43	10.09	8.46
Sep	12.8	0.73	−0.53	−0.32	11.48	8.79
Oct	7.1	0.65	−0.54	−0.26	12.93	11.50
Nov	2.9	0.67	−0.35	−0.26	14.21	16.08
Dec	−3.4	0.69	−0.25	−0.11	14.91	19.92

4. Synoptic patterns

Five key surface synoptic patterns were linked with the 143 radiation fog events at Albany during the 1970–79 period. Type 1 (Fig. 3a) is typified by a closed-isobar anticyclone where Albany is usually embedded within the first closed isobar (4 mb intervals). With the type 2 situation (Fig. 3b), an open ridge extends into the region (and usually over much of the northeast), often from a well-defined high pressure cell. Occasionally, mesoscale ridging follows a cold (or more often an occluded) front or trough passage, defining fog type 3 (Fig. 3c). Type 4 (Fig. 3d) occurs when a weak or dissipating frontal zone (frontolysis) is in the local vicinity, and type 5 (Fig. 3e) is associated with a col.

The monthly distribution of the radiation fog events associated with these five synoptic patterns is presented in Table 3. Type 1 is the dominant fog-forming situation accounting for just over 40% of all radiation fogs. Following in diminishing order of importance are type 2 (~22%), type 3 (~16%), type 4 (~12%), and type 5 (~9%). The closed high (type 1) and major ridge (type 2) situations often lead to "textbook" radiation fogs, where fog evolves in response to several nocturnal hours of light wind and mostly clear skies. Each of these two types shows an autumnal peak accounting for over 70% of their respective annual occurrences. Type 4 fogs also exhibit a peak in frequency (~68%) during the autumn months. Ridging behind a frontal zone or trough (type 3) and the col (type 5) tend to be less seasonally dependent, with the summer and fall months encompassing over two-thirds of these fogs. One could speculate that a higher initial relative humidity and warmer temperature associated with these fogs would allow for fog formation in less time [see Eq. (2)], lessening the importance of the limiting effect of the length of night.

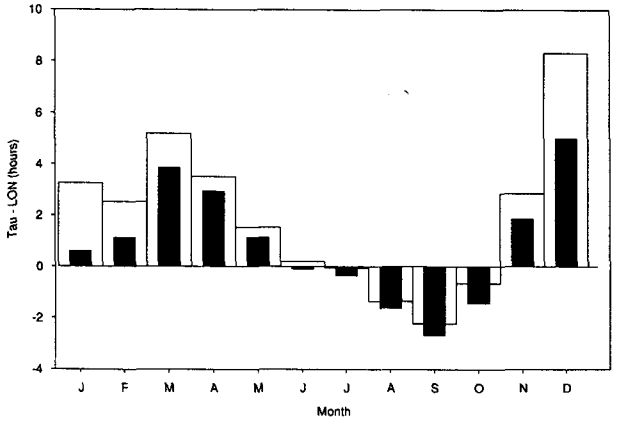

FIG. 2. Monthly distribution of the time (hours) necessary to reach saturation (τ) relative to the length of night (LON), τ–LON (black bars), and monthly distribution of the time necessary to produce condensation (τ_f) relative to the LON, τ_f–LON (white bars).

For the type 1 and 2 fog situations, location of the center (or ridge axis) of the surface anticyclone relative to the station location, appears to be an important factor (Table 4). A significant number (~47%) of these radiation fogs occur when the center of the high pressure cell or major ridge axis is situated over Albany. The position of the high pressure center or ridge east to southeast of the station also seems to be favorable for fog occurrence. This suggests that fog is less likely when the high pressure system is approaching from the west.

Table 5 introduces the averaged characteristics of the 143 radiation fog events by synoptic type. Each type 1, 2 and 5 radiation fog averages a little over 3 hours in duration, and in more than half of these cases visibility declined to what is arbitrarily defined as the "severe" fog level (visibility $\leq$ 100 m). These three surface synoptic patterns account for over 80% of severe radiation fogs at Albany. The fog severity ratio (FSR), defined as the ratio of the number of hours of severe fog to the number of hours of heavy fog, indicates that type 3 and 4 fogs are the least likely to produce periods of severe fog. Type 3 and 4 fogs also persist about 1 hour less, with only 17% and 33% of these events being severe, respectively. Additional SWOs, such as the vector-averaged wind speed, initial (at fog onset) pressure,

Unauthenticated | Downloaded 03/22/23 05:50 AM UTC

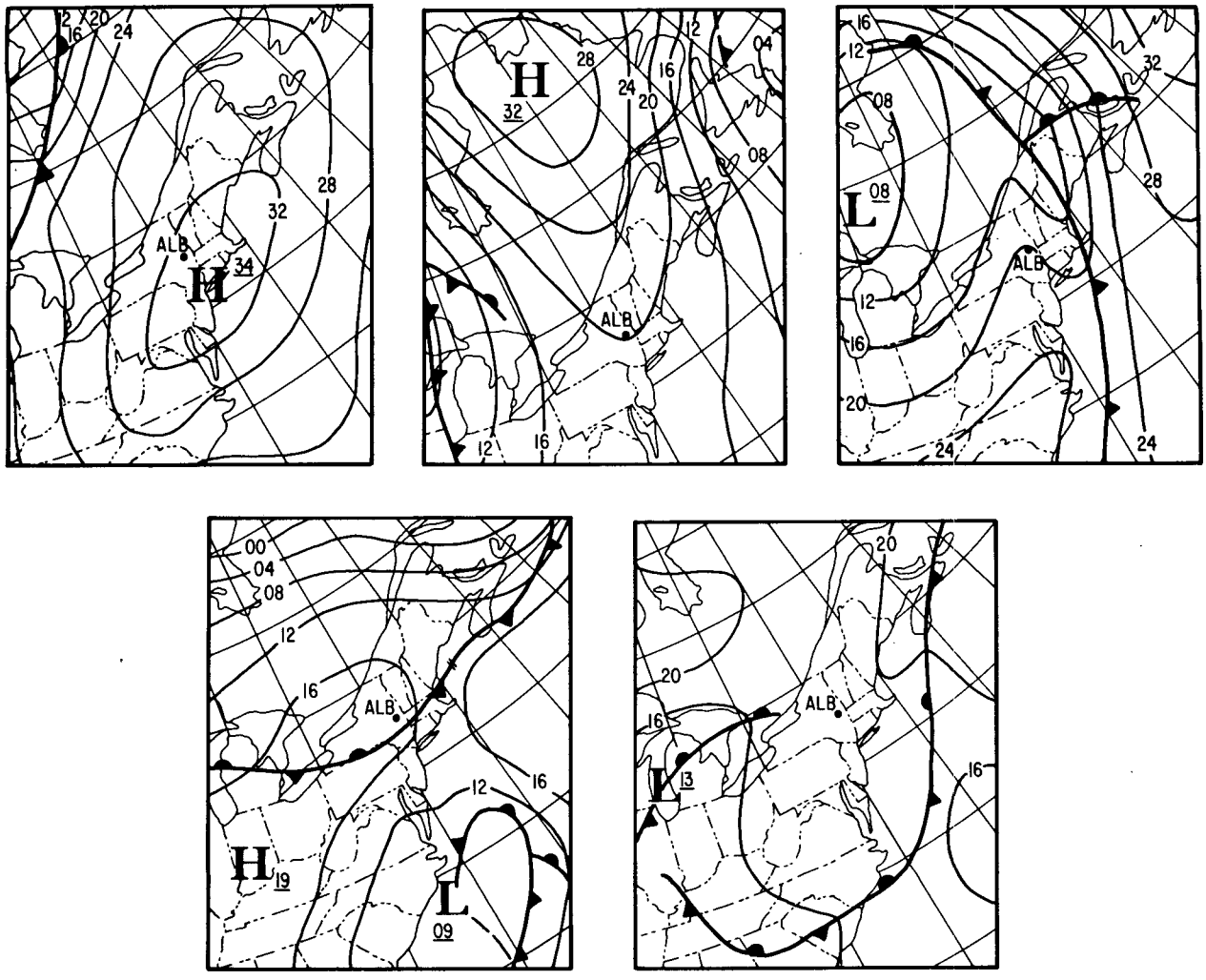

FIG. 3. Examples of surface synoptic patterns associated with heavy radiation fog events at Albany, New York, 1970–79. (a) Type 1—closed high (1200 UTC 26 September 1973), (b) type 2—major ridge (1200 UTC 3 October 1978), (c) type 3—postfrontal ridging (1200 UTC 3 April 1971), (d) type 4—weak front (1200 UTC 27 October 1977), (e) type 5—col (0600 UTC 31 July 1973).

and initial temperature, tend to reflect the nature of the synoptic situation. The surface pressure is higher when situated near the anticyclone center or ridge, while the lowest values are observed following front or trough passages. Lower initial temperature is linked to those situations most favorable for sustained periods of radiational cooling. As much as a 5 degree difference (warmer) is exhibited by the frontal types, most likely owing to restricted cooling by cloud cover or upper level moist layers for part of the evening. Wind speed is minimum (<1 m s^{-1}) for the dominant synoptic patterns (types 1 and 2).

TABLE 3. Monthly distribution of heavy radiation fog events by synoptic type (1970–79).

Type	Jan	Feb	Mar	Apr	May	Jun	Jul	Aug	Sep	Oct	Nov	Dec	Total
1	0	2	0	0	1	3	1	6	24	16	5	0	58
2	0	0	0	0	3	0	4	2	5	14	3	0	31
3	0	1	0	2	4	1	2	5	2	6	0	0	23
4	0	0	0	0	0	3	0	2	4	6	3	0	18
5	1	0	1	1	0	2	1	2	1	2	2	0	13
Total	1	3	1	3	8	9	8	17	36	44	13	0	143

Unauthenticated | Downloaded 03/22/23 05:50 AM UTC

TABLE 4. Surface high pressure center (Type 1) or major ridge axis (Type 2) location relative to Albany, New York.

Type	OC	N	NE	E	SE	S	SW	W	NW
1	20	4	6	11	5	5	3	2	2
2	22	0	0	2	5	1	0	1	0
Total	42	4	6	13	10	6	3	3	2

The prevailing vector-averaged wind directions during fog are calm (~40%), southerly (~20%), northerly (~15%), and northeasterly (~13%) (Table 6). These principal directions correlate well with the dominant high pressure location reported in Table 2. Furthermore, the northerly quadrant winds tend to be somewhat weaker then the winds from the south. "Fogging on a southerly wind" has been often noticed by local forecasters, and is probably due to the increasing influence of the pressure gradient after sunrise, and to some extent, funnelling through the north–south oriented Hudson Valley. Weaker northerly winds may be a consequence of a localized drainage flow in the valley in the absence of a significant pressure gradient.

An investigation of the role of measurable ($\geq$0.25 mm) precipitation prior to fog development indicates only a modest influence. Table 7 shows the percentage of fog events for which measurable precipitation was observed 12, 24, 48, and 72 hours prior to the onset of fog. Overall, less than one-third of fog events occur within 24 hours after measurable precipitation, and approximately one-half within 48 hours. For all synoptic fog types the percentage increases with time. This is more likely a result of the natural precession of synoptic systems. Note that type 3 fogs exhibit a greater tendency to form after precipitation due to the frontal or trough passage itself. Here, with shorter periods of radiational cooling usually observed in these postfrontal patterns, the additional initial moisture provided allows the fog formation process to occur in less time. Fog character showed little correlation with preceding precipitation measurements.

5. Diurnal characteristics

To reveal the diurnal nature of radiation fogs at Albany, the frequency of hourly radiation fog observations for our 143 fog events is plotted versus local standard time in Fig. 4. The graph shows a nearly monotonic increase in fog observations until a peak is reached between 0500 and 0600 LST. After 0700 LST, a rapid decline in fog occurrence is noted. From 1200 to 0000 there is, as expected, an insignificant contribution to the fog observations.

Recent radiation fog studies by Pilié et al. (1975), Roach et al. (1976), Mason (1982), and Meyer et al. (1986) indicate that increasing solar radiation associated with sunrise can act initially to promote, enhance and eventually dissipate radiation fog. The climatological data confirm this. Figure 5 shows the observations of radiation fog as given in Fig. 4, but now plotted relative to sunrise time. Also shown are the time of fog development and fog dissipation relative to sunrise time. Notice the peak in fog observations within the

TABLE 5. Averaged characteristics of heavy radiation fog events by synoptic type, 1970–79, Albany, New York. t_h (hh.mm) is the duration of heavy fog (in hours.minutes); N_s/N_h is the ratio of number of severe fog events to heavy fog events; FSR is the Fog Severity Ratio (see text); V_{min} [km] is the minimum visibility measured during fog event; U [m s^{-1}] is the average wind speed during fog event; P_o [mb] is the surface atmospheric pressure at fog onset; T_o [C] is the surface air temperature at fog onset. Standard deviation is noted in parentheses.

	Synoptic (fog) type					
	1	2	3	4	5	All
t_h (hh.mm)	3.09	3.24	1.58	2.46	3.07	2.58
	(3.10)	(2.12)	(1.55)	(2.10)	(2.52)	(2.40)
N_s/N_h	0.50	0.55	0.17	0.33	0.62	0.45
FSR	0.28	0.31	0.09	0.15	0.37	0.25
	(0.35)	(0.34)	(0.23)	(0.30)	(0.37)	(0.34)
V_{min} (km)	0.16	0.14	0.26	0.21	0.15	0.18
	(0.15)	(0.14)	(0.15)	(0.15)	(0.13)	(0.15)
U (m s^{-1})	0.73	0.91	1.32	1.60	1.54	1.05
	(0.90)	(0.95)	(1.32)	(1.40)	(1.03)	(1.11)
P_o (mb)	1025.6	1022.2	1014.4	1019.7	1017.4	1021.6
	(4.4)	(5.6)	(5.0)	(4.6)	(5.0)	(6.3)
T_o (°C)	7.4	7.5	12.1	11.8	10.0	9.1
	(4.3)	(5.4)	(4.8)	(5.0)	(6.4)	(5.3)

Unauthenticated | Downloaded 03/22/23 05:50 AM UTC

TABLE 6. Average wind speed (m s^{-1}) vs resultant wind direction per heavy radiation fog event, 1970–79, Albany, New York.

	Calm	N	NE	E	SE	S	SW	W	NW	Total
Calm	57	0	0	0	0	0	0	0	0	57
0.5–1.0	0	5	11	2	1	3	2	1	2	27
1.5–2.1	0	13	8	2	2	11	3	1	0	40
2.6–3.1	0	4	0	0	0	12	0	0	0	16
3.6–4.1	0	0	0	0	0	2	0	0	0	2
4.6–5.1	0	0	0	0	0	0	0	0	0	0
5.7–6.2	0	0	0	0	0	1	0	0	0	1
>6.2	0	0	0	0	0	0	0	0	0	0
Total	57	22	19	4	3	29	5	2	2	143

first hour after sunrise. Fog formation and dissipation also exhibit peaks within the hour before sunrise and within the second hour after sunrise, respectively. Based on median values, the radiation fog formation–dissipation cycle generally occurs in a 4 hour window centered about sunrise. Matveev (1967) reports similar findings from radiation fogs at the Zakharkovo Airport near Moscow, USSR.

The data presented above indicate that the time necessary for the cooling process to produce a fog is of the order of the length of night, thus confirming the physical model results from section 3b. Furthermore, some 23% of the fogs form after sunrise, suggesting that there exists a critical transition from the nocturnal saturation process to some mixing induced saturation coupled with lingering cooling. More important, however, is the role that sunrise plays in the dissipation of fog. The majority of fogs dissipate within three hours after sunrise. This is primarily due to increasing solar radiation helping to promote continued mixing through local heating, and to the entrainment of dryer air. So, while it takes many hours (on the order of the length of night) to form a radiation fog, only a few hours are required to dissipate it.

6. Some implications for fog forecasting

The possibility of radiation fog forming in the early morning hours need be considered only if one of the five surface synoptic patterns (discussed in section 4) is forecast (e.g., from the preceding day's 1200 UTC prognostic charts). In particular, a high pressure cell or ridge located directly over or to the east of Albany represents the most favorable synoptic situation. A preliminary assessment, using 1200 UTC surface weather maps during the Albany radiation fog season (September, October) for the period 1970–79, was made to estimate how often these synoptic patterns occur *without* fog development. The results indicate that 37% of the 175 observed type 1 (closed high) patterns produce fog. Thus, favorable synoptic situation is a necessary, but insufficient, precursor to radiation fog formation. The averaged meteorological characteristics associated with these synoptic patterns (see Table 4) enables us to better define the guidelines presented earlier (section 2) for identifying conditions most conducive for radiation fog formation. While a general need for clear (or clearing) skies, minimal wind speed, and falling air temperature was indicated, the climatological data show that wind speeds of under 1 m s^{-1} and temperatures cooling to the range of 2°–12°C are optimum for fog formation.

The physical model presented in section 3b explains that radiation fog at Albany, New York, is primarily a late-summer/early-autumn phenomenon, largely because the time necessary for the surface layer to saturate is shorter than the limiting length of night. Thus, one should not expect a high success rate for forecasts of radiation fog made outside of this fog season. The model also shows that the key parameters necessary for forecasting the onset time of fog are the initial relative humidity and cooling rate. Fog formation is favored under conditions of high initial relative humidity and strong nocturnal cooling. We believe that by applying this physical model on data from clear nights only, real probabilities of radiation fog formation could be assigned for a particular synoptic situation. This will be the focus of future work.

There are three central questions to the forecasting of fog: 1) When will the fog form? 2) How long will it last? 3) How severe will it be? Above, we have discussed

TABLE 7. Percentage of heavy radiation fog events following measurable precipitation, 1970–79, Albany, New York.

	Precipitation within:			
Type	12 hours	24 hours	48 hours	72 hours
1	0.0	13.8	41.4	60.3
2	0.0	22.6	45.2	51.6
3	47.8	82.6	87.0	91.3
4	16.7	27.8	38.9	61.1
5	23.1	23.1	53.8	69.2
All types	11.9	29.4	50.3	64.3

Unauthenticated | Downloaded 03/22/23 05:50 AM UTC

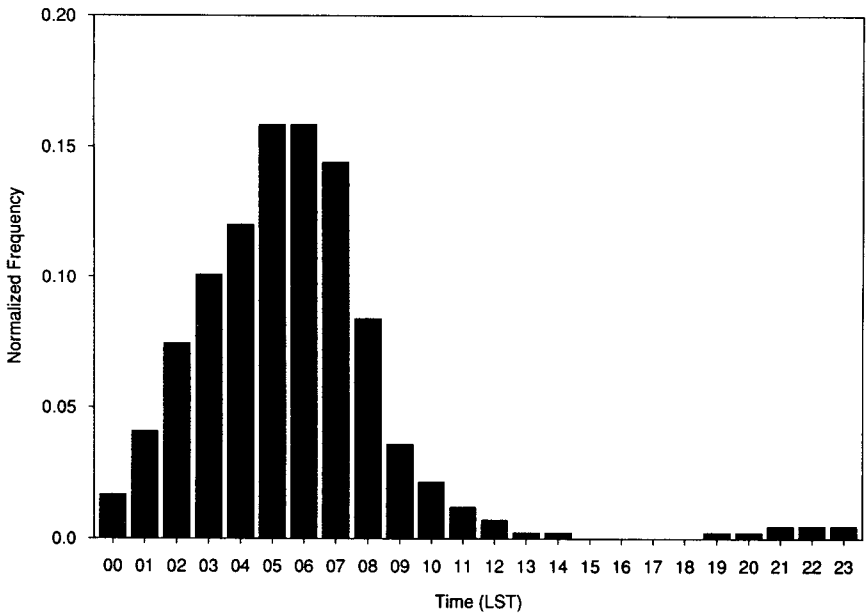

FIG. 4. Normalized frequency of hourly heavy radiation fog observations at Albany, New York, 1970–79.

how to address the first question, and our data have shown that most radiation fog forms within the 4 hours or so before sunrise. Additional refinement of the fog forecast requires specification of the fog character (e.g., duration, minimum visibility). We have shown that the longer duration fogs are associated with type 1, type 2, and type 5 synoptic patterns, and last an average of about 3 hours. The longer duration fogs also have a greater tendency to be accompanied by severe fog (visibility $\leq$ 100 m) conditions. Figure 6 shows a plot of the normalized frequency of heavy fog events (with and without observed periods of severe fog) versus fog event duration. The graph indicates that fogs lasting over 2 hours will have a higher probability of producing more restrictive visibility conditions.

The information gained in this work can be used

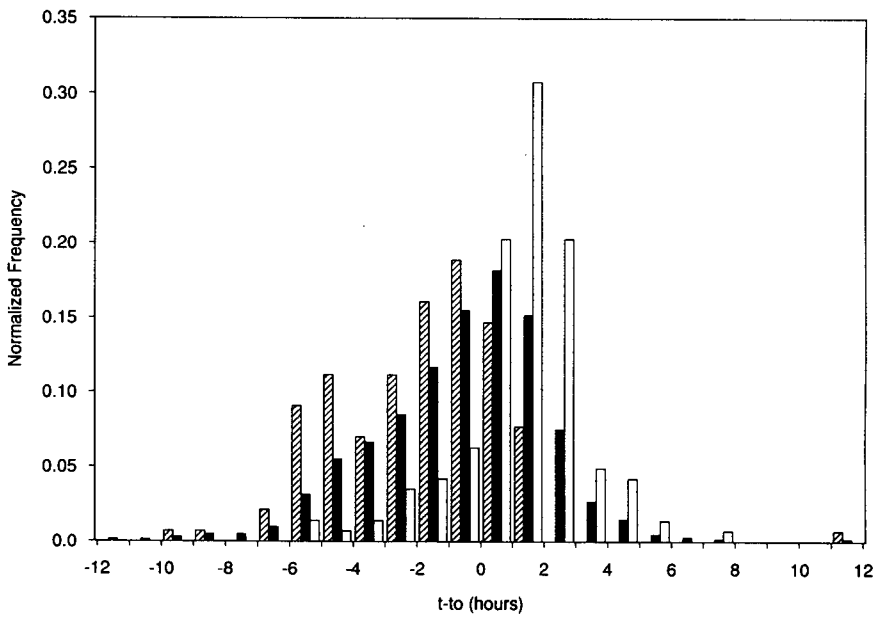

FIG. 5. Normalized frequency of hourly heavy radiation fog observations (black bars), time of fog formation (hatched bars), and time of fog dissipation (white bars) relative to sunrise time. Data are for Albany, New York, 1970–79.

Unauthenticated | Downloaded 03/22/23 05:50 AM UTC

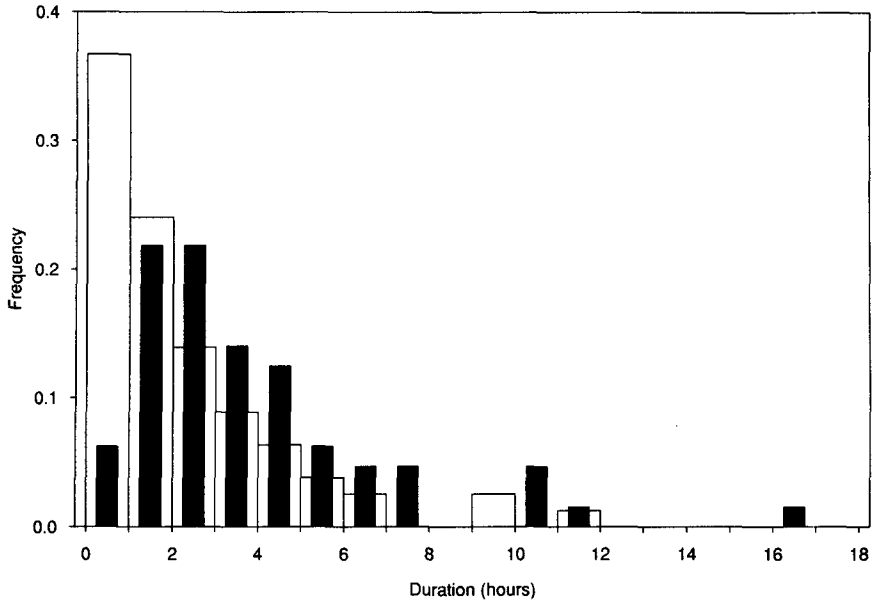

FIG. 6. Normalized frequency of heavy radiation fog events with (black bars) and without (white bars) periods of severe (visibility ≤ 100 m) fog versus fog event duration.

with confidence to practically eliminate a forecast of radiation fog for an obvious nonfog pattern. In general, we believe the weather analysis methodology developed, and some of the trends themselves, would apply to other inland regions of the northeastern United States.

Acknowledgments. This research has been supported by United States Army Research Office Grant DAAG2984K0050 and National Science Foundation Grant ATM8317455. David R. Fitzjarrald provided invaluable guidance with the preparation of this manuscript. We also appreciate the assistance of Cathy Hoefler, Dolores Leonard, Mark Kornfein, Marilyn Peacock and Paul Mausser along the way.

REFERENCES

Byers, H. R. 1959. *General Meteorology.* McGraw-Hill, 481 pp.

Court, A., and R. D. Gerston. 1966. Fog frequency in the United States. *Geogr. Rev.*, **56,** 543–550.

Emmons, G., and R. B. Montgomery. 1947. A note on the physics of fog formation. *J. Meteor.*, **4,** 206.

George, J. J. 1940. Fog: its causes and forecasting with special reference to eastern and southern United States. *Bull. Amer. Meteor. Soc.*, **21,** 135–148.

——, 1951. Fog. *Compendium of Meteorology,* T. F. Malone, Ed., Amer. Meteor. Soc., 1334 pp.

Hardwick, W. C. 1973. Monthly fog frequency in the continental United States. *Mon. Wea. Rev.*, **101,** 763–766.

Jiusto, J. E. 1981. Fog structure. *Clouds, Their Formation, Optical Properties, and Effect,* P. V. Hobbs and A. Deepak, Eds., Academic Press, 495 pp.

Mason, J. 1982. The physics of radiation fog. *J. Meteor. Soc. Japan,* **60,** 486–498.

Matveev, L. T. 1967. *Fundamentals of General Meteorology Physics of the Atmosphere.* Israel Program for Scientific Translations, Jerusalem. 699 pp. [NTIS# TT-67-51380.]

Meyer, M. B., J. E. Jiusto and G. G. Lala. 1986. FOG-82: A cooperative field study of radiation fog. *Bull. Amer. Meteor. Soc.*, **67,** 825–832.

Peace, R. L. 1969. Heavy-fog regions in the conterminous United States. *Mon. Wea. Rev.*, **97,** 116–123.

Petterssen, S. 1940. *Weather Analysis and Forecasting.* McGraw-Hill, 505 pp.

Pilié, R. J., E. J. Mack, W. C. Kocmond, W. J. Eadie and C. W. Rogers. 1975. The life cycle of valley fog. Part II: Fog microphysics. *J. Appl. Meteor.*, **14,** 364–374.

Roach, W. T., R. Brown, S. J. Caughey, J. A. Garland and C. J. Readings. 1976. The physics of radiation fog: I—a field study. *Quart. J. Roy. Meteor. Soc.*, **102,** 313–333.

Stone, R. G. 1936. Fog in the United States and adjacent regions. *Geogr. Rev.*, **26,** 111–134.

Taylor, G. I. 1917. The formation of fog and mist. *Quart. J. R. Meteor. Soc.*, **43,** 241–268.

Willett, H. C. 1928. Fog and haze, their causes, distribution, and forecasting. *Mon. Wea. Rev.*, **56,** 435–468.

——, 1944. *Descriptive Meteorology.* Academic Press, 310 pp.

Unauthenticated | Downloaded 03/22/23 05:50 AM UTC